Optics and Lasers in Engineering 158 (2022) 107157

Contents lists available at ScienceDirect

Optics and Lasers in Engineering

journal homepage: www.elsevier.com/locate/optlaseng

Comparative study of Shack-Hartmann configurations for atmospheric turbulence reconstructions in solar adaptive optics

Francisco García Riesgo[a,b,*], Sergio Luis Suárez Gómez[a,c], Jesús Daniel Santos Rodríguez[a,b], Carlos González Gutiérrez[a,d], Yolanda Martín Hernando[e], Luz María Montoya Martínez[e], Andrés Asensio Ramos[e], Manuel Collados Vera[e], Miguel Núñez Cagigal[e], Francisco Javier De Cos Juez[a,f]

[a] ICTEA (Instituto de Ciencias y Tecnologías Espaciales de Asturias), Spain
[b] Department of Physics, University of Oviedo, Spain
[c] Department of Mathematics, University of Oviedo, Spain
[d] Department of Computer Science, University of Oviedo, Spain
[e] IAC (Instituto Astrofísico de Canarias), Spain
[f] Department of Mining Exploitation and Prospecting, University of Oviedo, Spain

ARTICLE INFO

Keywords:
Adaptive optics
Artificial intelligence
Deep learning
Shack-Hartmann
Atmospheric turbulence
Neural networks
Fully-Convolutional Neural Networks

ABSTRACT

The correction of the phase variations induced by the atmospheric turbulence is one of the most complex problems that an Adaptive Optics (AO) System must deal with, as it must calculate the properties of all the atmosphere traversed by the light from several measures taken by ground-based telescopes. Traditional reconstructors systems used in AO are based on computational algorithms where its reconstruction quality improves with the number of measures made by the telescopes' sensors. That means that sensors are getting greater and greater with their corresponding higher financial expense. Artificial Intelligence (IA) has become in recent years a real alternative to traditional computational methods as reconstructors for AO systems. Fully-convolutional neural networks (FCNs) specifically have shown great performances working in Solar AO, demonstrating their ability to obtain a lot of valuable information from the recorded images for the wavefront phase evaluation. Along this research, the influence of the properties of the telescope's sensors and of the observations in the reconstructions made by the FCNs' is measured, to obtain the configuration that best suits the performance of artificial neural networks (ANN). The presented results determine the way forward for the future sensors for telescopes with reconstruction systems based on ANNs, to obtain higher quality reconstructions employing fewer economic resources.

1. Introduction

Telescopes have evolved from a simple combination of mirrors, lenses and crystals to a complex set of technology-improved systems working together, that pursuits a better understanding of the universe, by improving the quality of images from celestial bodies. amongst the most recent technologies, the improvements that some of these developments brought made those systems as Adaptive Optics (AO), engineering components, systems of sensors, etc. became necessary by its own merits.

AO is the field of optics whose aim is to correct in real time the distortions caused by the atmosphere in the received images on ground-based telescopes. In the last 30 years [1], with the improvement of computational systems, AO has experienced a tremendous development. Several AO systems were implemented in large ground-based telescopes and are still operating. On these telescopes, and on those planned for near-future implementation, rest the responsibility of the new discoveries that will be made during the next decades.

In the case of the technology for diurnal observation, its development for complex systems is still being researched since the majority of the telescopes that will perform solar observations in the upcoming years are still under construction, as the EST (European Solar Telescope) [2], a new four-metre class telescope. The development of these new large solar telescopes results on a new challenge for AO systems, they present new configurations as the Multi-Conjugate Adaptive Optics (MCAO) that implies that the amount of information to process in real time greatly

* Corresponding author at: ICTEA (Instituto de Ciencias y Tecnologías Espaciales de Asturias), Spain.
E-mail address: garciariefrancisco@uniovi.es (F.G. Riesgo).

https://doi.org/10.1016/j.optlaseng.2022.107157
Received 2 March 2022; Received in revised form 9 June 2022; Accepted 13 June 2022
Available online 24 June 2022

escalates in comparison with night-time AO systems. Some older solar telescopes with simpler configurations are currently using Solar AO systems, that are already well tested and implemented, as the one-metre class SST (Swedish Solar Telescope) [3,4] or the DST (Dunn Solar Telescope).

The field of Solar physics is less developed due to the extra difficulties involved in making daytime observations. The principal attractive is the Sun's atmosphere where many processes that affect live on Earth take place. amongst them, the most relevant are the Sun's luminosity variations, changing Earth's climate and how the magnetic fields are generated and dissipated in the Sun's atmosphere. It is necessary to obtain high quality images of the Sun's atmosphere and the Sun's surface to understand its activity.

The corrections made by Solar AO systems allow the telescopes to correct the aberrations suffered by the light on its way from the source to the telescope, obtaining a higher quality image; most aberrations are produced when the light passes throughout the Earth's atmosphere. The atmospheric turbulence is a random phenomenon that is continuously changing and producing aberrations on the wavefronts of the light. In a current AO system, there are some different parts that work together to obtain the corrected image. One of them is the Reconstructor System (RS) that is briefly introduced here since it is the focus of this research. When the light arrives at the telescope, measurements are made by several sensors that are sent to the RS to calculate an estimation of how the atmosphere was when the light passed through it. If it were completely known, the received image could be perfectly corrected with an ideal AO system.

In recent years, Artificial Intelligence (AI) methods have been applied in several scientific fields as mathematical tool that allows to simplify complex physical systems by numerical approximations, improving their performance. Artificial Neural Networks (ANNs) are one of the most developed fields in AI. Their good performance is well known in image recognition, language processing, image classification, etc. [5,6]. Several science branches have taken advantage of these improvements and ANNs are currently applied in diverse areas, such as prediction systems, car industry to make self-sufficient cars, simulation platforms of diverse nature, etc. AO is one of the fields where ANNs have been applied showing a great performance in night observations, as the CARMEN reconstructor [7–9].

In this research a new reconstructor system (RS) is presented for extended images, particularized to solar observations, based on Fully-Convolutional Neural Networks (FCNs), a type of ANN characterized by its good performance working with images. The main objective of the research is to establish a comparison of how the reconstruction changes depending on the variations of some parameters of the AO system; the number of subapertures of the Shack-Hartmann wavefront sensor, the number of pixels of each subaperture and the field of view of the observation are the ones compared. The properties of FCNs allow to obtain reconstructions working with simpler AO sensors than the ones currently used, requiring Shack-Hartmann wavefront sensors with less subapertures and pixels per subaperture, that will imply lower economic contributions and a simpler control.

This manuscript is composed by 4 more sections; the material and methods section consist in a description of the main concepts of adaptive optics, Shack-Hartmann wavefront sensor, the simulation platform used to generate the data and artificial intelligence, explaining how the problem can be solved with their use. Next, the architecture and some parameters of the FCN used are detailed in the Section 3, showing the results of the RS and their discussion in Section 4. Finally, some conclusions and future developments are presented in the last section.

2. Material and methods

In this section an introduction to the main concepts of Solar adaptive optics and artificial neural networks is presented.

2.1. Solar adaptive optics (Solar AO)

The term Adaptive Optics comprehends a set of techniques whose aim is the real-time correction of the images received by ground-based telescopes. Aberrations are present in the images formed of celestial bodies causing that the quality of the images decreases considerably. The principal source of aberrations is the atmospheric turbulence existing in the part of the way where the light travels through the Earth's atmosphere.

The Earth's atmosphere consists of multiple air masses of several sizes and shapes that are in constant relative in movement. Each one has its own properties: size, wind's direction and velocity, temperature, height, etc. The relative movements between the air masses, like fluids movements, cause the atmospheric turbulence to be a random phenomenon in constant change, which makes the work of AO systems difficult to reach real time corrections, without knowing how the turbulence will be in the next moment. The turbulence of larger scales is passed to turbulences at lower scales [10]. The air masses are commonly represented as turbulence layers at different heights, so the path that light makes through the atmosphere consists of passing through several turbulence layers, each one with its own refraction index value. The way that the light goes through the atmosphere to the telescope can be modelled as it has traversed a path with multiple lenses of various refraction indexes, one after the other [1].

Corrections performed by an AO system are made after the light is received by the telescope, before it is observed. The system must do several processes that includes to sense the image, to reconstruct the estimated atmospheric turbulence that the light has traversed and finally with the previous information to calculate the corrections to apply, to eliminate as much aberration effects as possible.

As it was commented before, the air masses of the turbulence are grouped by layers. According to the Kolmogorov's model [10] when describing a turbulence layer there are two main parameters, its height, and its intensity that is given by the Fried's coherence length (commonly designated as r_0) [11]. The physical interpretation given to r_0 corresponds to the diameter of a telescope that, in absence of turbulence, offers the same resolution as a large telescope in presence of that specific atmosphere. So, the lower r_0 value, the higher turbulence intensity; r_0 is commonly given in centimetres, where 12 cm represents a worse day for observation where the turbulence has high intensity and values between 15–18 cm represents a normal day for observation. An extremely bad turbulence condition is represented when r_0 is lower than 10 cm, under these circumstances an observation would usually be suspended.

Another important parameter when performing an observation is the Field of View (FOV). This value represents the maximum angular size of the object as seen from the entrance pupil. Commonly the FOV is determined by the field over which the optical system exhibits good performance.

There are several AO Systems according to its configuration. However, they usually have the same components; at least one Wavefront Sensor (WFS) where the aberrations presented in the received wavefront are measured, a Reconstructor System (RS) which estimates how the atmosphere is at each moment and calculates a correction for the aberrations and at least one Deformable Mirror (DM) that consists in a mirror which surface can be modified where the received wavefront is reflected and is applicated to it the corrections calculated by the RS. In this work an SCAO system was chosen (Simple Conjugate Adaptive Optics). It is the simplest system in AO since it has one WFS and one DM on-axis with the celestial body working on close loop (see Fig. 1).

The reconstructors that are usually used nowadays in AO Systems are based on matrix vector multiplication applying least squares methods or minimum variance techniques [12–14]. In the last years some reconstructors based on ANNs have been successful in night AO systems, as the CARMEN reconstructor or the CARMEN Convolutional reconstructor [15]. The work presented is an evolution of these last kind of reconstructors but in this case applied for Solar observations.

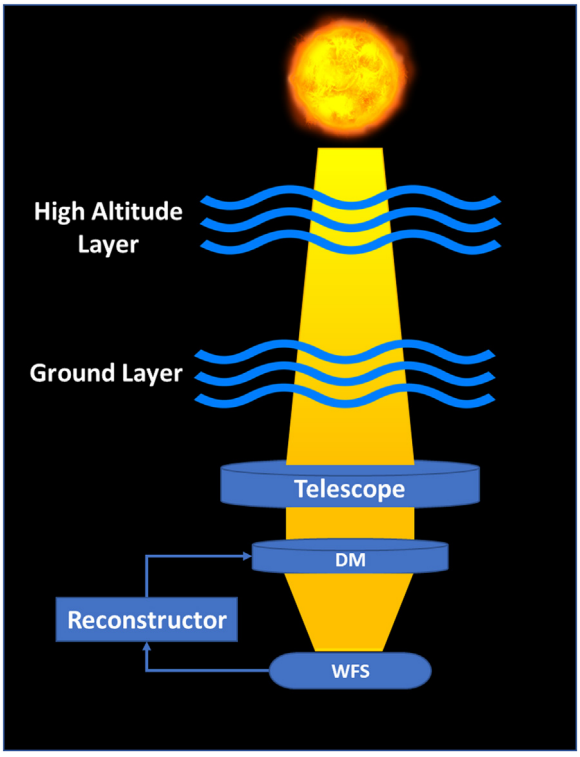

Fig. 1. Schematic representation of a Solar SCAO configuration.

There are several difficulties when making a Solar observation compared with a night one, for the AO system. These are the most important:

- First, the Sun is an extended object when it is observed from Earth since it is much nearer than any other star. Therefore, the telescope's pupil and all the subaperture pixels of the SH are completely saturated by the Sun's surface (see Fig. 2) instead having only a spot of light in the centre. The SH must commonly make some preprocessing on the data received before passing it to the RS.
- In diurnal observations, due to the solar energy emitted, the atmospheric turbulence has more intensity, implying higher turbulences than at night hours. It is expected then that the r_0 is lower at day.
- Solar AO must work in the visible spectral range while night systems tend to work in the infrared where both sensing and correction are easier.
- Some alternative wavefront reconstruction algorithms have been developed for night time astronomy.

2.1.1. Shack-Hartmann wavefront sensor

The Shack-Hartmann (SH) is the most used WFS in Adaptive Optics both in night and solar observations, and the one chosen in this work. It is composed of a matrix of lenses with the same focal length, being focalised each one in a different subaperture. The subapertures are located after the lenses, composed by another matrix of separated CCDs (charge-coupled device) or other photon sensors. Each lens focalises the received light on its corresponding subaperture. In an ideal situation, the light of the celestial body would be received as a plane wavefront that, after passing through the lens, will be focalized in the centre of each subaperture, being equal for all of them. Due to the presence of the atmospheric turbulence, the wavefront presents aberrations that can be calculated by the comparison of the images received by the subapertures.

The SH divides the wavefront in discrete sub-pupils and process the data before passing them to the RS. It calculates cross-correlations [16] between the images received by each subaperture, the number can be limited to reduce the time needed. Then, the maximum of the cross-correlations is located for each subaperture. The SH is able to obtain from that value the gradient or tilt of each subaperture [17]. The gradient is usually used by commonly RS as the Least-Square method.

The principal difference between the reconstructors based on convolutional neural networks and the others resides on the property of CNNs of using images as inputs. The images received by each subaperture are directly used as input of the RS and the pre-processing data procedure made by the SH is not necessary, avoiding the loss of information and the time needed.

The most common reconstructor systems used nowadays in real telescopes are based in the Least-Squares reconstruction method (LS). When using this reconstructor, the result will be better the more subapertures the sensor has. Nevertheless, the maximum number of subapertures is limited by the diameter of the pupil and the cost of the sensor depends on them, being higher when the number of subapertures increases. For this reason, it is interesting to obtain new reconstructors that can achieve good reconstructions even with a low number of subapertures. The other parameter that has influence on the information received is the number of pixels per subaperture, that represents the number photon sensors that the SH has in each subaperture.

2.2. Fully-convolutional neural networks

Artificial Neural Networks are an interconnected group of processing units, that tries to mimic the behaviour of biological neural networks [18]. These structures are characterized for being able to learn from the data and give an answer to a determinate problem. They are formed by individual computational units, called neurons. The neurons are sorted in different layers, forming a neural structure. The output of one layer is the input of the neurons of the next layer since neurons are linked to those from the previous and following layer. These connections are regulated by weights whose values can be modified during the training process.

The training process is the method that allows an ANN to learn from the data and takes place before the ANN is used. Each neuron applies an activation function over the input given by the previous ones. The process consists of the application of the network to a train dataset that its correct outputs are known. Then, using algorithms that measure the error, the ANN is adjusted to minimize the error of the outputs of train dataset varying some parameters, as the connections weights until the error is decreased to a minimum value. The most used algorithm is the backpropagation algorithm [19] and it is the one used in this work.

The kind of neural networks selected is the Fully-Convolutional Neural Networks (FCNs) [20,21] that are based on Convolutional Neural Networks. An FCN consists in several layers of neurons joined in two blocks, a convolutional block and a deconvolutional block (see Figs. 3 and 4). That allows having both input and output data as a multidimensional array. The convolutional block can be formed by several convolutional layers and pooling layers. The convolutional layers work as filters extracting the main features of the input given. The pooling layers reduce the size of the input by selecting the most significant value over a group of pixels, which is chosen by a set criterion, being the maximum value usually selected. In this work no pooling layers were used; the size of the input was reduced by using convolutional layers with strides size higher than one pixel. At the end of the convolutional block, the features are fussed in the deconvolutional section until obtain the final image as output. This deconvolutional block usually is formed by deconvolutional and transpose pooling layers.

For the case of this research, the input data given to the FCNs are the images of wavefronts received by the SH (as the right image of the Fig. 2) obtaining as output the profile of the turbulence phase for each moment (as it is represented in the schemes of Figs. 3 and 4).

During a common training process, a train dataset is passed through the FCN with input images and their desired outputs are known. The error is backpropagated through the different layers to be minimized. The filters of the layers and the weights of the connections are modified

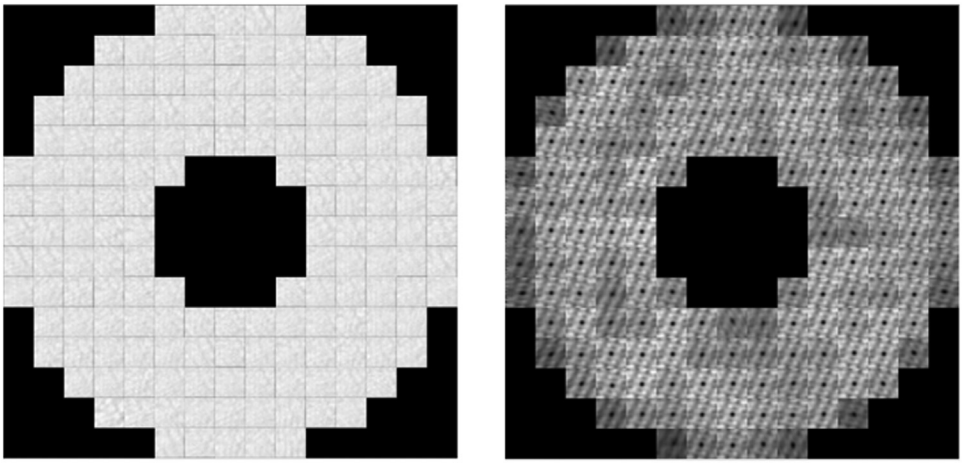

Fig. 2. Example of the information received by an SH of 15 × 15 subapertures. On the left, there is an image of the information received without any pre-processing. On the right, the same information after the cross-correlations have been made by the SH.

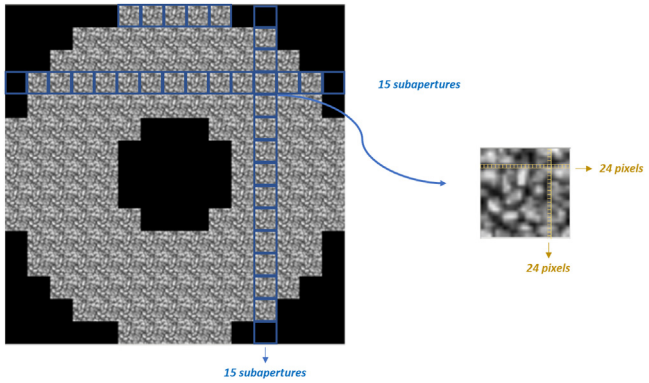

Fig. 3. Description of the main parameters compared in an example of input image. The squares in blue represent the subapertures in the SH image and the ones in yellow the pixels over each subaperture.

with the backpropagation, each time that the error is backpropagated they are updated. The network is applied to the dataset several times to train it, being the number of times that it is passed selected by the user. In the experimental setup section, the main characteristics of the neural networks topologies and the datasets used are detailed.

2.3. DASP: durham adaptive optics simulation platform

All the dataset used for the training, validation and test processes were simulated using THE Durham Adaptive optics Simulation Platform (DASP) [22]. DASP tries to mimic the data obtained in real telescopes, allowing to make simulations in diurnal or nocturnal observations. In the case of diurnal ones, it only can replicate an SCAO AO system or a MCAO one. SCAO was the chosen one for this research.

The atmospheric turbulence is generated according to the Von-Karman statics implemented with Monte-Carlo Simulations [10]. The incident wavefront phase is aberrated with several thin perturbed layers, DASP simulates it agreeing to the previously chosen setup and generates the image of the SH as a convolution of Sun's surface image with the generated turbulence layers.

The platform allows the user to select multiple parameters of the simulation. For each case, a parameter file is needed that specify relevant ones, dimension the system and determines the output to be produced [22]. In the case of this research, these parameters include amongst others the Fried's coherence length (r_0), the outer scale (L_0), the height of each layer, the wind velocity and the direction of each layer and the contribution of each layer to the total turbulence. Further, much information can be extracted from the simulation, as the information received by the SH, the correlations, the phase of the turbulence, the DM position, etc. In the datasets simulated for the research only the SH images and the image of the turbulence's phase has been saved, whose constitute the input and the output of the FCNs. The base of the simulated SH images is a synthetic solar granulation image of the Sun's surface with a resolution of 0.0139″/pixel All the datasets used both for training, testing and validation were simulated with this platform.

2.4. Experimental setup

The experiments were performed with an Ubuntu LTS 14.04.3 server, which has 128Gb of DDR4 memory, Nvidia GeForce GTX TitanX, an Intel Xeon CPU E5–1650 v3 @ 3.50 GHz and SSD hard drive. As computer language, Python was chosen for its performance with packages of Artifi-

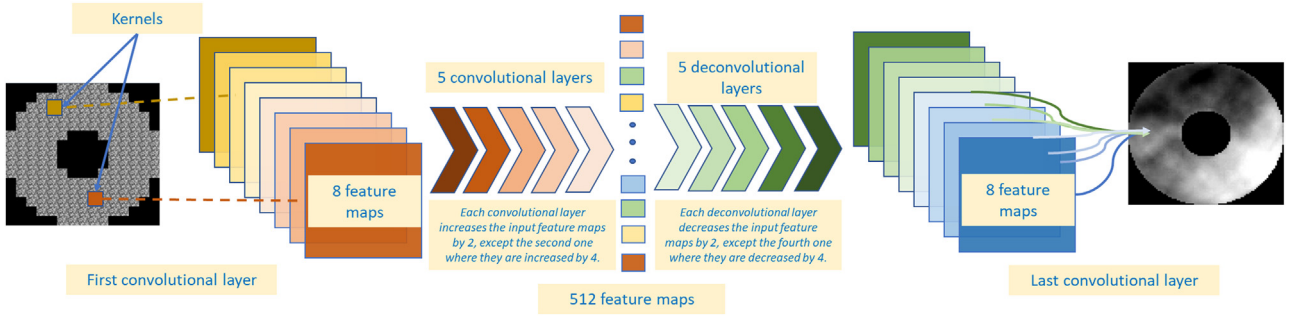

Fig. 4. Schematic representation of an FCNs selected. Due to the number of layers, it corresponds with the Model 1, 2 and 3 since the differences between them are the kernels size and the strides of the layers.

Table 1
Shack-Hartmann configurations used to compare the influence of the number of subapertures. Values correspond with the number of pixels per side, assuming that images of the subapertures and of the phase of the turbulence have a square shape. The table is divided to indicate the cases where the two neural network models were used.

	15×15 subapertures	10×10 subapertures	7×7 subapertures	3×3 subapertures
Pixels per subaperture	24×24	36×36	48×48	112×112
Total pixels of the Shack-Hartmann	360×360	360×360	336×336	336×336
Total number of pixels of the phase	90×90	90×90	84×84	84×84
FCN model	Model 1		Model 2	

cial Intelligence as Tensorflow 2 [23] and Keras [24]. Also, the adaptive optics simulator DASP [22] is written with Python 2.

Different simulations were generated for the training, validation and test process of the FCNs. The influence of three different parameters in the reconstruction was studied, these parameters are: the number of subapertures, the number of pixels per subaperture and the FOV of the observation. For each, one train dataset, one dataset for validation and three test datasets were simulated. The simulations presented are based on the SCAO configuration of the Gregor Solar Telescope [25], with 1.5 m optical aperture . Furthermore, each dataset has the same number of images to allow a realistic comparison: train sets had 80,000 while each test dataset had 6000 images. One sun region was set for all the obtained images. Results are shown in the next section, calculated as the mean value over the 6000 simulations.

Considering the parameters of each set, they are as follows: the train dataset consisted of 80,000 simulated images. Each simulation had two different turbulence layers, the first one is always situated at 0 m of height and had a weight of the 10% over all the atmospheric turbulence. The other layer was set at different heights, varying from 0 to 20,000 m in steps of 200 m of height and having the remaining 90% of the weight. That structure of the dataset giving the 90% of weight to the second layer allows to train the network for several heights' turbulence layers. The r0 value ranged from 8 cm, where the turbulence is stronger, to 16 cm per each altitude simulated in steps of 1 cm. For each case, 100 different situations were created. So, 100 steps of height by 8 steps of r_0 value by 100 samples for each situation gives in the total the 80,000 simulated images. The validation dataset consisted of 6000 simulated images where the turbulence layer varied from 0 m to 15,000 m of height in steps of 1000 m, having the same weight as in the previous case. The r_0 value ranged from 8 to 16 cm per altitude in steps of 1 cm. For this dataset 50 simulations were made for each configuration.

The three test datasets were simulated with an atmospheric turbulence with the same layers structure as the explained before, excepting the heights' step, it was modified being the test one of 500 m of altitude. The r_0 value was set the same value for all the simulations of the set.

Once the shared parameters of the simulations for all the studies have been described, the own features of the FCNs and the datasets of simulations used for each one are detailed in the next subsections. Several FCNs with different topologies were tested before the ones selected for each case. The input parameters of the FCNs, presented differences for each case studied, that could be quantified as 5 times bigger of the inputs size, from the smallest to the biggest case considered, which prevented the use of a single topology of the FCN.

2.4.1. Influence of the number of subapertures

For the analysis of the influence of the number of subapertures, four SH configurations were employed, with 15×15, 10×10, 7×7 and 3×3 subapertures, respectively. To compare the influence of the subapertures, we keep constant the total number of pixels of the input image. The configurations of the SH compared are shown in the Table 1.

Two different topologies of FCNs were used for the four cases as is showed in Table 1, since there were two possible inputs shapes 360×360 and 336×336 pixels. The total number of pixels, the number of subapertures, the number of pixels per subaperture and the total number of pixels of the phase image must satisfy some relations according to the DASP simulation platform to carry out the simulation [22]. Only few combinations are allowed so they were selected to obtain the final input shape as similar as possible to perform the most reliable comparison, giving rise in the two input shapes mentioned above.

The first two cases used the same network as the input shape was 360×360 pixels in both, and another one was used for the last two with an input shape of 336×336 pixels:

- The Model 1 is formed by a convolutional block with 6 layers with kernels of size 11×11, 7×7, 5×5, 5×5, 3×3 and 3×3, respectively without pooling layers, and a deconvolutional block that is formed by another 6 layers with kernels 3×3 and the rest 5 layers, 5×5, respectively. Padding is added in all the layers and the hyperbolic tangent is used as activation function. The input image is reduced from 360×360 to 5×5 pixels in the convolutional block by using strides of shape 2×2 or 3×3. Then the image is increased to its final shape of 90×90 pixels by the deconvolutional block by using strides of shape 2×2 and 3×3.
- The Model 2 is similar to the first one in all the parameters, except on the strides of the layers. In this case, the input image is reduced from 336×336 to 7×7 by using strides of shape 2×2 and 3×3 and then the image is increased to 84×84 pixels with strides of shape 3×3 and 2×2.

2.4.2. Influence of the number of pixels

New datasets were simulated to analyze the influence of the number of pixels per subaperture. They all consist in three subapertures and the same FOV but varying the total number of pixels. All the configurations selected are shown in Table 2.

To check the performance on the simplest configuration of the previous subsections, 3 subapertures were chosen. The first case selected is 3×3 subapertures with 112×112 pixels per subaperture, where the datasets from the previous point were used and it allow us to reuse the FCN that had shown a good performance. This selection outnumbers the usual configuration used in a real SH, so it was considered the biggest case as the other ones had less pixels; 48×48 and 28×28, respectively.

Unlike the previous subsection, for this case a unique model of FCN with its own topology was made for each configuration; the simulated images were so different in size terms so the same network could not be used, as it could only be optimized for one of the situations. The selected models are explained behind:

- Model 2 is the same as the used in the previous experiment with the same name as the datasets are the same too. To sum up, it consists in an FCN with 6 convolutional layers and 6 deconvolutional layers without pooling layers.
- Model 3 is similar to the first one, but the kernels and strides of the layers were modified according to the new input and output sizes of the images. It is composed by the same number of layers, with kernels of size 9×9, 7×7, 5×5 and all the last ones with size 3×3, respectively for the convolutional block. The deconvolutional block is formed by 6 deconvolutional layers with kernels of size 3×3 for the first layer and 5×5 for the rest. Images are reduced from 144×144 pixels to 3×3 pixels using strides of size 2×2 and 3×3 and then an increase is made to obtain outputs of 36×36 pixels of phase by using strides in the deconvolutional block of the same shape. Hyperbolic

Table 2
Shack-Hartmann configurations used to compare the influence of the number of pixels per subaperture.

PIxels per subaperture	112 × 112 pixels	48 × 48 pixels	28 × 28 pixels
Total Pixels of the SH	336 × 336	144 × 114	84 × 84
Total number of pixels of the phase	84 × 84	36 × 36	21 × 21
fcn model	Model 2	Model 3	Model 4

Table 3
Shack-Hartmann configurations used to compare the influence of the FOV. All the simulations that have been made for previous comparisons were remade with 10 arcseconds of FOV. The FCN's models correspond with the ones used in previous studies.

	15 × 15 subapertures	10 × 10 subapertures	7 × 7 subapertures		3 × 3*subapertures*	
Pixels per subaperture	20 × 20	28 × 28	42 × 42	24 × 24	48 × 48	96 × 96
Total number of pixels of the SH	300 × 300	280 × 280	294 × 294	72 × 72	144 × 144	288 × 288
Total number of pixels of the phase	75 × 75	70 × 70	77 × 77	18 × 18	36 × 36	69 × 69
	Model 1	Model 2	Model 3	Model 4		

tangent function is used as activation function as in the previous models.

- The Model 4 is the smallest, since the input image had size of 84 × 84 pixels. Model 4 is composed by 5 convolutional layers, so only one less layer than the others, and kernels of size 9 × 9, 7 × 7, 5 × 5, 3 × 3 and 3 × 3, respectively, followed by 4 deconvolutional layers with kernels 3 × 3 the first one and 5 × 5 all the rest. In this case the input image is reduced to 7 × 7 pixels by applying strides of size 2 × 2 and 3 × 3. Then, it is increased by the deconvolutional block by using strides of 3 × 3pixels in the second layer. The activation function selected for this case is the hyperbolic tangent function.

2.4.3. Influence of the FOV

New simulations were generated to determine the influence of the FOV of the observation. All the previous studies were made with simulations of 6 arcseconds of FOV. So, to take advantage of the previous results, all the simulations were remade with 10 arcseconds as it allowed us to compare case by case the influence of the FOV with the previous selected configurations.

The FCNs used to evaluate the influence of the FOV were the same as in previous subsections for each case. Due to the limitations of the DASP simulator, the shape of the FCN's inputs was different to previous cases as they had to obey some relations between the FOV, the number of pixels and the number of subapertures. Anyway, we decided to maintain the characteristics of the FCNs to make a realistic comparison since the simulations were similar enough in terms of the inputs shape to allow us to use the same topology. The configurations of the simulations are shown in Table 3 with the chosen model of FCN from each one.

The test datasets used in the comparison had the same characteristics as in the previous situations, they were formed by 3 datasets for each simulation, having fixed r_0 values of 8, 10 and 12 cm each one.

2.5. Residual WFE

The residual RMSE WFE is the chosen magnitude to evaluate the quality of the reconstructions. The residual WFE allows to measure how similar are two pictures by calculating the RMSE of the difference pixel by pixel of both images. In this case, as the images correspond to the turbulence's phase, it is expressed in wavelengths units. The surface obtained by the difference pixel by pixel of two identical images has a zero residual WFE value, as it increases, the difference between images also increases. The error can be calculated as follows:

$$\text{residual WFE} = \sqrt{\frac{\sum_{i=1}^{N}(x_i - y_i)^2}{N}}$$

Being x_i the pixels of the original image, y_i the reconstructed ones and N the total number of pixels of both images.

The residual WFE is often presented in radians, in those cases it is calculated as:

$$\text{residual WFE (rad)} = \frac{2\pi}{\lambda} * \sqrt{\frac{\sum_{i=1}^{N}(x_i - y_i)^2}{N}}$$

Where λ represents the wavelength of the incoming light.

3. Results and discussion

The results are divided in three subsections, to show the three objectives of the research: the influence of the number of subapertures, the number of pixels per subaperture and the FOV of the observation.

Results from all the cases are given considering the mean of value of the residual WFE and with the percentage of the similarity between the phase reconstructed by the FCN and the original phase, the one simu-

Table 4
Comparison of the influence of the variation on the number of subapertures. The most turbulent layer for each case is shadowed in light grey, whose intensity increases as the intensity of the turbulence decreases.

Subapertures	r0(cm)	Residual WFE (nm)	Similarity (%)	WFE original (nm)	WFE Network (nm)
15	**8**	304.79	72	621.52	445.65
	10	235.56	80	516.47	411.43
	12	206.91	85	443.26	376.41
10	**8**	249.88	91	526.82	477.48
	10	206.11	94	437.63	410.63
	12	180.65	96	375.62	359.7
7	**8**	204.52	93	662.9	615.95
	10	155.18	96	550.69	526.82
	12	101.07	97	472.7	458.38
3	**8**	202.93	91	684.39	623.91
	10	146.43	96	568.2	542.73
	12	93.90	94	499.76	471.11

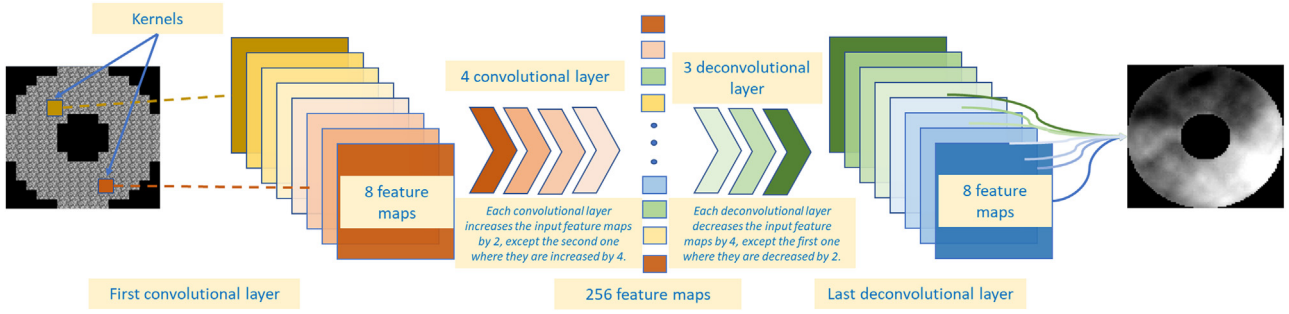

Fig. 5. Schematic representation of the topology of the FCN selected as Model 4. The difference between the other models apart from the sizes of their kernels and strides is that Model 4 has one less convolutional layer and only four deconvolutional layers.

lated by DASP. Some figures of the reconstructed and the original phase are also shown for a visual comparison.

3.1. Influence of the number of subapertures

In Table 4 the quality of the reconstructions performed by the FCN for each SH's configuration for different intensity of turbulence layers is compared. Note that all the r0 values are very low, so the best situation with 12 cm of r0 is still a significantly turbulent situation. It is expected, then, that errors obtained were high even the reconstructor made a well performance. An example of the reconstruction made by the FCN is shown in Fig. 5.

The results show that the networks improve the quality of the reconstructions when the number of subapertures decreases. There also exists a clear trend in the similarity of the reconstructions, which increases from 72% to 93% when the subapertures are reduced from 15×15 to 7×7, less than a half, at high atmosphere turbulence conditions. Also, note that 15×15 subapertures is a number that could be found perfectly in a reconstructor system of a solar telescope of 1.5 m of pupil, as the one selected in the simulations.

Another important parameter that has not been mentioned yet is the time taken by the network to perform the reconstruction. For the cases showed above, practically there are not differences being always the mean computational time needed per sample over each test under 4.6 ms. The test that showed the lowest value was the one that considers 7 subapertures one with r_0 value of 10 cm, where the recall time mean value over that test was 4.43 ms. The slowest one was 10 subapertures with 8 cm of r_0 that needs 4.54 ms per sample.

Therefore, models 1 and 2 show similar execution times, being the second one slightly faster since its inputs are smaller than those of the first model.

When using FCNs, all the information of the image given as input is analyzed, instead of using the standard SH method, where only 2 values, the slope information, can be recovered from each subaperture. This is an advantage because no information of the input is lost. That fact allows the FCNs to achieve good performance in the reconstructions without a high number of subapertures. Furthermore, the input of the FCN is the complete image with all the subapertures, where there are abrupt changes in the boundaries of the subapertures since each one is saturated by the Sun's image (see Fig. 2). These limits are misunderstood by the FCN causing that the system achieves better reconstructions with less subapertures, contrary to the working of other reconstruction methods.

The trend mentioned before is not saw when the results for 7×7 and 3×3 subapertures are considered. Despite with 7×7subapertures there are more subaperture's limits, the information received by an SH with only 3×3 subapertures in total is not enough to reconstruct the turbulence's phase in its all regions, as the FCN does not have enough information of the aberrations received due to not have sufficient subapertures to compare them.

Moreover, the less is the intensity of the turbulence, the higher is the similarity of the reconstruction with the original image. All the cases correspond with extreme conditions, especially $r_0 = 8cm$. So, it is expected that under lighter circumstances it would work better. That fact is very interesting for close loop adaptive optic systems, as the images received are firstly corrected with the information of the aberrations of the previous moment before being received by the WFS, so the intensity of the aberrations measured by the SH are much slower.

3.2. Influence of the number of pixels

The quality of the reconstructions was measured using three test datasets with the same characteristics as in the first study, with r_0 values of 8, 10 and 12 cm each one. Results are shown in Table 5.

The importance of the number of subapertures lies in the information received from the SH. The higher number of pixels, the more information extracted by the FCN. Consequently, the phase may be reconstructed with more precision. In the cases of high values of r_0, the atmosphere is more uniform, so reconstructions can be made even having low number of pixels.

Table 5
Results of the comparison of the influence of the variation on the number of pixels per subaperture. The most turbulence layer for each case is coloured in light grey, and the colour becomes more intense as the intensity of the turbulence decreases.

Pixel per subap.	r0(cm)	Residual WFE (nm)	Similarity (%)	WFE original (nm)	WFE Network (nm)
112	**8**	208.50	91	684.39	619.93
	10	151.20	95	568.20	541.94
	12	130.51	94	499.76	471.11
48	**8**	179.85	89	634.25	567.40
	10	126.53	97	526.02	510.90
	12	105.05	98	452.01	444.85
24	**8**	213.27	84	615.15	518.06
	10	124.94	97	510.11	494.19
	12	101.07	99	438.48	432.91

Table 6
Results obtained for reconstructions made with simulations with 10 arcseconds of FOV. All the simulations of previous subsections were remade with 10 arcseconds to compare case by case the influence of the FOV with the previous selected configurations.

Subapertures	Pixel per subaperture	r0(cm)	Residual WFE (nm)	Similarity (%)	WFE original (nm)	WFE Network (nm)
15	**20**	**8**	217.25	88	591.28	518.06
		10	167.12	96	491.01	472.70
		12	147.22	97	421.77	432.12
10	**28**	**8**	257.04	88	666.88	587.30
		10	190.20	94	553.88	522.04
		12	165.53	96	475.89	457.58
7	**42**	**8**	222.82	93	635.84	592.07
		10	175.08	95	528.41	503.74
		12	150.41	97	453.60	439.28
3	**96**	**8**	154.38	94	582.52	547.51
		10	112.21	97	483.85	468.73
		12	94.70	98	415.41	405.86
	48	**8**	164.73	93	637.43	590.48
		10	118.57	97	529.21	512.49
		12	98.68	98	454.40	444.06
	24	**8**	139.26	91	650.17	592.87
		10	77.99	97	539.55	530.80
		12	59.68	98	463.15	458.38

Analysing the results; they show that the quality of reconstructions made by ANNs is influenced positively by the total number of pixels of the SH, as expected. In Table 5 can be seen how the original phase and the one retrieved by the FCN are more similar when using higher number of pixels, especially in the cases of worst turbulence conditions. For r_0 values of 12 cm, there is practically no difference when varying the number of pixels between 122 per subaperture and 24, but it is expected that if the number of subapertures is reduced even more, the similarity will decrease, as the amount of information received by the FCN may not be enough. However, when the r_0 value represents high turbulence conditions, as $r_0 = 8$ cm, it is seen how the quality of the reconstruction decreases around 7% between the case with more subapertures in comparison to the one with less subapertures.

As in the previous subsection the computational time needed was also analyzed for the 3 ANN models. Every value given is calculated as the mean time needed per sample over all the tests. The ANN Model 3 was applied for the case with 48×48 pixels per subaperture, obtaining a mean computational time of 4.41 ms, 4.39 ms, and 4.43 ms for 8 cm, 10 cm and 12 cm of r_0, respectively. The ANN Model 4 was applied for the last case with 24×24 pixels per subaperture, the mean times needed per sample were 4.18, 4.22 and 4.23 ms for 8, 10 and 12 cm of r_0.

Comparing these results with the previous subsection the only case that showed an improvement in terms of computational time is the 24×24 pixels per subaperture one, being approximately 4% faster than the big one of 112×112 pixels per subaperture. It may be due to the smaller size of the input images or to the topology of the ANN model, as Model 4 is composed by one less convolutional and deconvolutional layer. From this study can be concluded that the number of layers of the ANN model affects the computational time, since the intermediate case of 48×48 pixels per subaperture obtains similar computational times to the bigger one, despite being half the size.

3.3. Influence of the FOV of the observation

The influence of the FOV in the reconstructions made by FCNs is analyzed comparing the results obtained with 10 arcseconds of FOV with the results obtained in previous subsections, all of them obtained over simulations with 6 arcseconds of FOV. The quality of the reconstructions made with the new datasets can be seen in Table 6 as the results obtained with 6 arcseconds of FOV are shown in Tables 4 and 5.

To analyze the results, the cases with 8 cm of r_0 are principally commented since they are where most differences are obtained. Beginning with the case with most subapertures, for an SH of 15×15 subapertures the similarity of the reconstruction is improved from 72% with 6 arcseconds of FOV to 88% with 10 arcseconds when using the same FCN model. It should be noted that in the new simulations, the number of pixels per subaperture has been reduced from 28 to 20 due to DASP simulator relations. A better reconstruction is obtained even initially having a worse situation. To sum up, in this case increasing the FOV of the simulation from 6 arcseconds to 10, the quality of the reconstruction has improved a 16% even reducing the number of pixels per subaperture, which implies worse reconstructions as it has been discussed in the previous subsection.

In the case of 20 subapertures, the result has decreased from 91% to 89% but as before, the number total of pixels of the SH with 10 arcseconds of FOV was 280 versus the 360 pixels with 6 arcseconds of FOV, in this case the worse result is attributed to the reduction of the number of pixels. So, if the quality of reconstructions is almost the same despite that great difference in pixels, it is possible to reaffirm that the FCN reconstruct better with higher values of FOV.

As results of 7 subapertures shows there are practically no differences between the two situations. It is expected that the reconstruction will improve for the FCN in this case since it is made with less pixels per subapertures again, 42 versus 48, that suppose in total 294 vs 336.

In the cases made with SH of 3 subapertures the same tendency is observed, as for all the cases a better reconstruction is retrieved, even in the biggest one, where despite having 16 pixels less per subaperture (a 14% less), the similarity is improved from 91% to 93% for an r_0 value of 8 cm.

Finally, from situations with r_0 values higher than 8 cm, the quality of the reconstructions is approximately the same with 6 or 10 arcseconds. In some cases, as in the last one with 3 subapertures, the similarity is even higher for the situations with 10 arcseconds. So, in conditions of normal intensity turbulence, the new reconstructor can achieve phases of the turbulence closer to the original ones in simulations with 10 arcseconds of FOV despite having less pixels per subaperture.

4. Conclusions

A new reconstructor system for Solar AO based on FCNs has been tested throughout this paper. The influence on its reconstructions of some observation's parameters as the number of subapertures of the SH, the number of pixels per subaperture and the FOV of the observation has been studied to know the benefits of the new reconstructor and how the most suitable configurations are (Fig. 6).

The first conclusion that can be extracted from the study is that a better reconstruction is not due to have more subapertures as happens with commonly used reconstructor systems in Solar AO. The FCN only

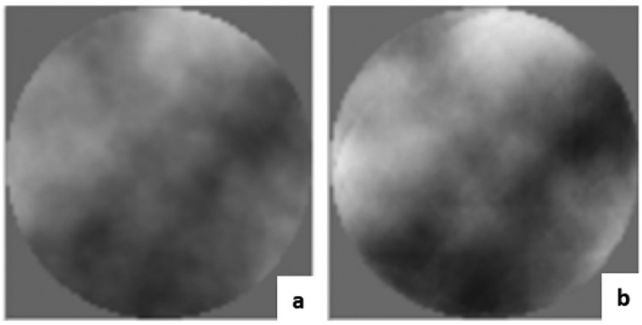

Fig. 6. Example of the reconstruction made by the FCN for a 7 × 7 subapertures SH. Fig. 5.a represents the original image (simulated with the DASP simulator) and Fig. 5.b the final reconstructed phase obtained by the FCN. It corresponds to a situation of r0 = 8 cm. It is important to note how the reconstructed phase has approximately the same shape, having the turbulence in the same region of the image, as the original one.

Table 7
Configuration with best results obtained from the cases studied. A higher optimized configuration can be modelled using the results extracted from each of the cases studied.

Parameters with best results from the cases evaluated in the study		
Number of subapertures	**Pixels per subaperture**	**FOV**
7 × 7	42 × 42	10

need enough subapertures to interpret the turbulence in the different regions of the pupil but, from that number on, stems to the characteristics of Solar observations, the FCN misunderstands the information received and the quality of the reconstructions decreases. In our study the most adequate number was 7 × 7 subapertures.

In previous works made by our group, we had obtained that LS working with an SH with these characteristics obtains a mean similarity in the reconstructions of 85% over a dataset of 6.000 images for r_0 values of 8 cm. Consequently, it is important to highlight that our new reconstructor improves the reconstructions an 8% in terms of similarity using SHs with less than a half subapertures than the most used one.

From the second study made, it can be concluded that the number of pixels per subaperture of the SH favourably affects to the quality of the reconstruction made. As all the information received is used by the FCNs, the higher number of pixels have the subapertures, the better reconstructions will make the ANN. Having more pixels implies that the FCN receives more information of the atmosphere turbulence conditions at each moment. That fact becomes more important in worse atmospheric turbulence situations, where the biggest differences in the similarity of the reconstructions can be seen from the study. Anyway, in economic terms, it is more interesting to increase the number of pixels per subaperture than the subapertures of the Shack-Hartmann.

On the other hand, increasing the number of pixels implies more computational time for the reconstructions if that means growth the number of layers of the topology of the ANN. However, variations in computational time are not relevant as the maximum difference appreciated was a 4% and for all the cases ANNs have showed very competitive times of execution, being always lower than 4.6 ms.

Finally, the last research provides that the FCNs achieves better results in observations when the FOV is higher. The higher FOV in the observation, the more similar reconstructions made. In the situations studied through that subsection, the FCN got similar results between 6 and 10 arcseconds of FOV or even better with 10 arcseconds despite using in the last case simulations with less pixels per subaperture. In Table 7 is presented the configuration that has shown the best results from the cases studied.

The final subsection allows us to confirm the conclusions obtained in the previous research, as all the simulations of them were remade with 10 arcseconds of FOV for it. The trends observed of the influence of the number of subapertures and of the number of pixels per subaperture were also fulfilled in this subsection.

The r_0 values used for testing the FCNs is something that should be noted, since all of them represents bad turbulence conditions, especially the cases with 8 cm as it is associated with extremely bad conditions. Seeing the trend of all the cases studied, the similarity increases with the r_0 value, so it can be expected that the quality of the reconstructions improves under normal viewing conditions.

Future developments of this research will consist of apply the ANNs in an optical bench or a telescope, to verify that the conclusions drawn are still valid working with real data. Furthermore, the reconstructor could be developed for more complex AO systems, as the MCAO one since they are the most used currently in solar telescopes.

Declaration of Competing Interest

The authors declare that they have no known competing financial interests or personal relationships that could have appeared to influence the work reported in this paper.

CRediT authorship contribution statement

Francisco García Riesgo: Methodology, Investigation, Software, Writing – original draft. **Sergio Luis Suárez Gómez:** Conceptualization, Data curation, Writing – review & editing. **Jesús Daniel Santos Rodríguez:** Methodology, Writing – review & editing. **Carlos González Gutiérrez:** Conceptualization, Software. **Yolanda Martín Hernando:** Software. **Luz María Montoya Martínez:** Visualization, Conceptualization, Writing – review & editing. **Andrés Asensio Ramos:** Methodology, Validation, Writing – review & editing. **Manuel Collados Vera:** Supervision, Writing – review & editing. **Miguel Núñez Cagigal:** Conceptualization, Writing – review & editing. **Francisco Javier De Cos Juez:** Visualization, Writing – review & editing, Supervision.

References

[1] Tyson R. Principles of adaptive optics. CRC Press; 2010.
[2] Collados M, et al. European solar telescope: progress status. Astron Nachr 2010;331(6):609–14.
[3] Scharmer GB, Dettori PM, Lofdahl MG, Shand M. In: Keil SL, Avakyan SV, editors. Innovative Telescopes and Instrumentation for Solar Astrophysics, 4853. Bellingham, WA, USA: Society of Photo Optical; 2003. p. 370–81.
[4] Scharmer GB, Bjelksjo K, Korhonen TK, Lindberg B, Petterson B. In: Keil SL, Avakyan SV, editors. Innovative Telescopes and Instrumentation for Solar Astrophysics, 4853. Bellingham, WA, USA: Society of Photo Optical; 2003. p. 341–51.
[5] Mirowski PW, LeCun Y, Madhavan D, Kuzniecky R. Comparing SVM and convolutional networks for epileptic seizure prediction from intracranial EEG. In: Proceedings of the IEEE workshop on machine learning for signal processing; 2008. p. 244–9.
[6] Nagi J, et al. Max-pooling convolutional neural networks for vision-based hand gesture recognition. In: Proceedings of the IEEE international conference on signal and image processing applications (ICSIPA); 2011. p. 342–7.
[7] Osborn J, et al. Open-loop tomography with artificial neural networks on CANARY: on-sky results. Mon Not R Astron Soc 2014;441(3):2508–14.
[8] Gómez SLS, Gutiérrez CG, Rodríguez JDS, Rodríguez MLS, Lasheras FS, de Cos Juez FJ. Analysing the performance of a tomographic reconstructor with different neural networks frameworks. Adv Intell Syst Comput 2017;557:1051–60.
[9] Osborn J, et al. First on-sky results of a neural network based tomographic reconstructor: carmen on Canary. Adaptive Optics Systems IV, 9148. SPIE; 2014. 91484M p. 1541–6.
[10] Zilberman A, Golbraikh E, Kopeika NS. Propagation of electromagnetic waves in Kolmogorov and non-Kolmogorov atmospheric turbulence: three-layer altitude model. Appl Opt 2008;47(34):6385–91.
[11] Rimmele TR. Solar adaptive optics. Adapt Opt Syst Technol 2000;4007:218–32.
[12] Rimmele TR, Marino J. Solar adaptive optics. Living Rev Sol Phys 2011;8(1):2.
[13] Ellerbroek BL. First-order performance evaluation of adaptive-optics systems for atmospheric-turbulence compensation in extended-field-of-view astronomical telescopes. JOSA A 1994;11(2):783–805.
[14] Roggemann MC. Optical performance of fully and partially compensated adaptive optics systems using least-squares and minimum variance phase reconstructors. Comput Electr Eng 1992;18(6):451–66.
[15] Riesgo FG, Gómez SLS, Lasheras FS, Gutiérrez CG, San Cristóbal CP, de Cos Juez FJ. Convolutional CARMEN: tomographic Reconstruction for Night Observation. In:

Pérez García H, Sánchez González L, Castejón Limas M, Quintián Pardo H, Corchado Rodríguez E, editors. Proceedings of the international conference on hybrid artificial intelligence systems. Lecture Notes in Computer Science, 11734. Springer; 2019. p. 335–45.
[16] Berkefeld T. Solar adaptive optics. In: Kneer Franz, Puschmann Klaus, Witman Axel, editors. Modern solar facilities-advanced solar science. Proceedings of a Workshop Held at Gottingen, September 27-29. Universitätsverlag Göttingen; 2007. p. 107–13.
[17] Knutsson PA, Owner-Petersen M, Dainty C. Extended object wavefront sensing based on the correlation spectrum phase. Opt Express 2005;13(23):9527–36.
[18] Gardner MW, Dorling SR. Artificial neural networks (the multilayer perceptron)—a review of applications in the atmospheric sciences. Atmos Environ 1998;32(14):2627–36.
[19] Goodfellow I, Bengio Y, Courville A, Bengio Y. Deep learning, 1. MIT Press Cambridge; 2016.
[20] García Riesgo F, et al. Early fully-convolutional approach to wavefront imaging on solar adaptive optics simulations. In: Proceedings of the international conference on hybrid artificial intelligence systems; 2020. p. 674–85.
[21] Shelhamer E, Long J, Darrell T. Fully Convolutional Networks for Semantic Segmentation. IEEE Trans. Pattern Anal. Mach. Intell. 2017;39(4):640–51.
[22] Basden AG, Bharmal NA, Jenkins D, Morris TJ, Osborn J, Peng J, et al. The Durham Adaptive Optics Simulation Platform (DASP): Current status. SoftwareX 2018;7:63–9.
[23] Abadi M, et al. TensorFlow: a system for large-scale machine learning. OSDI 2016;16:265–83.
[24] Gulli A, Pal S. Deep learning with keras. Packt Publishing Ltd; 2017.
[25] Berkefeld T, Schmidt D, Soltau D, von der Lühe O, Heidecke F. The GREGOR adaptive optics system. Astron Nachr Nov 2012;333(9):863–71.